THE ASTROPHYSICAL JOURNAL, 335:269–289, 1988 December 1

RESONANCE LINE POLARIZATION IN SPHERICAL ATMOSPHERES

K. N. NAGENDRA
Indian Institute of Astrophysics
Received 1987 December 14; accepted 1988 May 17

ABSTRACT

The problem of resonance line polarization is studied using simple theoretical models. The medium is assumed to be a finite slab or a finite spherical shell-like atmosphere. The atmosphere is assumed to be at rest in the present paper. The atmospheric extension of the spherical atmospheres is also taken to be small. Both these aspects will be discussed in a future publication. The main purpose of this paper is to understand the behavior of line polarization in spherical media, in analogy with plane-parallel situation. Hence only schematic atmospheric models are employed for the sake of clarity. The atmospheric models could represent possibly the photospheric layers of giant stars. The line center optical depths employed by us correspond to the photospheric weak absorption lines. A comparison of lines formed under complete redistribution (CRD) and partial redistribution (PRD) in frequency is presented, for both plane-parallel and spherically symmetric media. The dependence of the resonance line polarization on physical parameters of the two-level atom formulation, and on the global parameters such as extendedness, the opacity law in a spherical medium, and the boundary conditions are studied. The resonance line polarization by coherent scattering (CS) is also discussed. A rough estimate of the distribution of line intensity and line polarization across the spherical disk of a moderately extended spherical atmosphere is presented, through an example.

Subject headings: line formation — polarization — radiative transfer

I. INTRODUCTION

The basic theory of resonance line polarization and its diagnostic potential in solar observations have been explored in a series of papers by Stenflo and his coworkers (Stenflo 1976; Stenflo and Stenholm 1976; Stenflo, Bauer, and Elmore 1980). Dumont, Omont, and Pecker (1973), and Auer, Rees, and Stenflo (1980) have computed polarization profiles assuming coherent scattering to explain observations in the line wings. The importance of partial frequency redistribution (PRD) effects in the resonance line polarization was shown by Dumont *et al.* (1977) and Rees and Saliba (1982). McKenna (1984, 1985) has computed line polarization using various partial redistribution functions and realistic model atmospheres. Faurobert (1987, 1988) has discussed the validity and usefulness of some approximate forms of the $R_{\text{II-A}}$ frequency redistribution function in the polarized line transfer computations, in relation to the exact angle-dependent version of this function. This well-known redistribution function represents the resonance line scattering mechanism in a two-level atom model. In the works mentioned above, always the plane-parallel radiative transfer equation of the problem is solved. This paper is concerned with a study of the same problem using the transfer equation for a spherically symmetric system. A comparison is made with plane-parallel (PP) solutions. The net polarization of light emitted by a spherical star, however, is identically zero. Our final aim is to use the spherically symmetric (SS) radiative transfer solutions to calculate the polarization of light emitted by rotationally and/or tidally distorted extended atmospheres of stars. In this paper we have just shown some important characteristics of the SS solutions of the resonance line polarization transfer problem. The scalar PRD resonance line formation in SS systems has been well studied (e.g., Mihalas 1978 for details and a list of references to earlier works). In selecting the SS atmospheric models for theoretical computations we have been guided by the well-known paper of Kunasz and Hummer (1974). We have used the Peraiah-Grant method (Peraiah 1984) for solving the spherical radiative transfer problem.

The polarization in a resonance line arises due to coherent scattering by an atom in its own rest frame. Such a two-level atom model is a quantum analog of the Rayleigh scattering of the continuum radiation. The general theory of the scattering mechanism for full Stokes vector including the effect of magnetic fields has been discussed by Landi degl'Innocenti (1984), where references to earlier work could be found. The resonance line polarization is sensitive to the magnetic field (Hanle effect), the collisional rates, interference between atomic sublevels, the frequency redistribution model (CRD, PRD, or coherent scattering [CS]), the degree of angular anisotropy of the incident radiation, and finally the geometry of the line-forming region. It is only with this last effect that we are mainly concerned here. The $R_{\text{II-A}}(x, x')$ in Hummer's standard notation is used for PRD computations. The Voigt profile is always used as the profile function. The redistribution function is directly evaluated and the usual hybrid model suggested by Rees and Saliba (1982) is employed in incorporating this function into the (2×2) polarization scattering phase matrix for resonance line polarization (Chandrasekhar 1960). In this hybrid model the angular anisotropy in the scattering process is retained only in the scattering phase matrix, and the frequency redistribution is represented by the conventional scalar function which is introduced as a multiplier to the angular terms in the phase matrix (e.g., Rees and Saliba 1982; Faurobert 1987). Faurobert (1987, 1988) however, has used the full angle-dependent redistribution matrix $R_{\text{II}}(x, \mu, x', \mu')$ and has shown that the hybrid model, which is widely used, is a good approximation in practice.

In the next section we present the relevant equations. In the third section we give some general information about the method of solution and the model parametrization. In the fourth section we discuss the results. Each subsection in the fourth section is self-contained and aimed at presenting the role of a particular physical parameter in the line formation process. Specific conclusions are drawn at the end of each subsection. The general features of the study are summarized in § V.

II. THE SPHERICALLY SYMMETRIC RADIATIVE TRANSFER EQUATIONS FOR RESONANCE LINE POLARIZATION

Because of the axial symmetry of the radiation field in both PP and SS geometries, the Stokes parameters I_l and I_r are sufficient to represent the polarization state of the radiation field. $I = I_l + I_r$ and $Q = I_l - I_r$ are the equivalent set of Stokes parameters to I_l and I_r. The quantity I is the usual specific intensity of the scalar transfer equation. The degree of linear polarization $p = Q/I$ is a measure of the anisotropy of the diffuse radiation field. The sign convention is that a positive value of p corresponds to a polarization directed perpendicular to the surface. The transfer equation is written below for a two-component vector $\boldsymbol{I} = (I_l I_r)^{\mathrm{T}}$. It is a vector analog of standard non–LTE two-level atom line transfer equation. The equation of transfer in spherical symmetry is given by

$$\mu \frac{\partial}{\partial r} \boldsymbol{U}(x, \mu, r) + \frac{1-\mu^2}{r} \frac{\partial}{\partial \mu} \boldsymbol{U}(x, \mu, r) = k^L[\beta + \phi(x)][\boldsymbol{S}(x, \mu, r) - \boldsymbol{U}(x, \mu, r)] , \tag{1}$$

where $\boldsymbol{U}(x, \mu, r)$ is the Stokes specific intensity vector at an angle $\theta = \cos^{-1} \mu (\mu \in [0, 1])$ to the symmetry axis (radius) at the radial point r in the atmosphere, and the reduced frequency point $x = (\nu - \nu_0)/\Delta\nu_{\mathrm{D}}$ in the line. The quantity ν is the frequency of the radiation in Hz at any frequency point in the line; ν_0 is the line center frequency, and $\Delta\nu_{\mathrm{D}}$ is the Doppler width which is assumed to remain constant throughout the atmosphere. The quantity β is the ratio k^C/k^L of opacity due to continuous absorption per unit interval of x to that in the line, and k^L is the frequency integrated line opacity. The optical depth scale is given by $d\tau(r) = -k^L(r)dr$. Throughout we have used the conventional notation and for the sake of economy, the number of arguments inside the right most brackets is restricted. In general, each one of the physical quantity in equation (1) can be an arbitrary function of variables x, μ, and r. The normalized absorption profile is represented by a Voigt function

$$\phi(x) = H(a, x)/\sqrt{\pi} , \tag{2}$$

with the Voigt a parameter representing a constant value of damping width to the Doppler width. The specific intensity vector in spherical symmetry is defined by

$$\boldsymbol{U}(x, \mu, r) = 4\pi r^2 \boldsymbol{I}(x, \mu, r) . \tag{3}$$

The source vector is given by

$$\boldsymbol{S}(x, \mu, r) = \frac{\phi(x)\boldsymbol{S}^L(x, \mu, r) + \beta \boldsymbol{S}^C(r)}{\beta + \phi(x)} ; \tag{4}$$

$\boldsymbol{S}^L$ and $\boldsymbol{S}^C$ refer to the source functions in the line and continuum, respectively, where

$$\boldsymbol{S}^C(r) = \tfrac{1}{2} B'(r)\mathbf{1} , \qquad \mathbf{1} = (1, 1)^{\mathrm{T}} , \tag{5}$$

is the unpolarized continuum source vector. The source vectors for the I and Q Stokes parameters are defined by

$$S_I(x, \mu, r) = \left[\frac{\phi(x)}{\beta + \phi(x)}\right][S_l^L(x, \mu, r) + S_r^L(x, \mu, r)] + \left[\frac{\beta}{\beta + \phi(x)}\right][B'(r)] , \tag{6}$$

and

$$S_Q(x, \mu, r) = \left[\frac{\phi(x)}{\beta + \phi(x)}\right][S_l^L(x, \mu, r) - S_r^L(x, \mu, r)] . \tag{7}$$

Defining

$$\eta(x) = \frac{\phi(x)}{\beta + \phi(x)} , \qquad 1 - \eta(x) = \frac{\beta}{\beta + \phi(x)} , \tag{8}$$

the equations (6) and (7) can be rewritten as

$$S_I(x, \mu, r) = \eta(x) S_I^L(x, \mu, r) + [1 - \eta(x)]B'(r) , \tag{9}$$

and

$$S_Q(x, \mu, r) = \eta(x) S_Q^L(x, \mu, r) . \tag{10}$$

The quantity $\eta(x)$ has a frequency dependence similar to that of the profile function in the line core region ($x \lesssim 3$). However, for the large values of β we have employed in this paper—representing a strong unpolarized continuum radiation superposed on the partially polarized pure line radiation—the frequency independent β increasingly influences the $\eta(x)$ behavior in the far wings. As a result, the "unpolarized" continuum source function $\boldsymbol{S}^C(r)$ dominates the partially linearly polarized line source function in the wings, thus gradually driving the linear polarization in the wings to zero. The line source vector is given by

$$\boldsymbol{S}^L(x, \mu, r) = \begin{bmatrix} S_l^L(x, \mu, r) \\ S_r^L(x, \mu, r) \end{bmatrix} = \frac{(1-\epsilon)}{\phi(x)} \int_{-\infty}^{+\infty} dx' \int_{-1}^{+1} \boldsymbol{R}(x, \mu, x', \mu') \boldsymbol{U}(x', \mu', r) d\mu' + \frac{\epsilon}{2} B'(r)\mathbf{1} , \tag{11}$$

where ϵ is the probability per scatter that a photon is destroyed by collisional de-excitation. The redistribution matrix $\boldsymbol{R}(x, \mu, x', \mu')$

accounts for the correlations in frequency, direction, and polarization state that exists between the incident photon characterized by (x', μ') and the reemitted photon characterized by (x, μ), during a scattering event involving a two-level atom and the incident and reemitted photons. This matrix is defined in the form

$$\boldsymbol{R}(x, \mu, x', \mu') = \boldsymbol{P}(\mu, \mu')R(x, x') . \tag{12}$$

The phase matrix for resonance scattering is given by

$$\boldsymbol{P}(\mu, \mu') = \frac{3}{8} E_1 \begin{bmatrix} 2(1-\mu^2)(1-\mu'^2) + \mu^2\mu'^2 & \mu^2 \\ \mu'^2 & 1 \end{bmatrix} + \frac{(1-E_1)}{4} \begin{bmatrix} 1 & 1 \\ 1 & 1 \end{bmatrix} . \tag{13}$$

The factor $(1 - E_1)$ measures the amount of depolarization. It depends on the angular momentum quantum numbers j_l and j_u of the transition involved (l = lower state, u = upper state). A maximum polarization occurs for $(j_l = 0) \rightarrow (j_u = 1)$ type transitions (e.g., the Ca I 4227 Å resonance line) where $E_1 = 1$. In such a case $\boldsymbol{P}(\mu, \mu')$ reduces to the Rayleigh scattering phase matrix (see Chandrasekhar 1960 for details). We have always employed $E_1 \equiv 1$. The quantity $R(x, x')$ in equation (12) is an angle-averaged redistribution matrix. A good discussion about separating out frequency and angle dependence as implied in equation (12) is given in Faurobert (1987). The following are the redistribution functions used in this paper.

CS:

$$R(x, x') = \delta(x' - x)\phi(x') , \tag{14}$$

CRD:

$$R(x, x') = \phi(x)\phi(x') , \tag{15}$$

PRD:

$$R(x, x') = R_{\text{II-A}}(x, x') , \tag{16}$$

with

$$R_{\text{II-A}}(x, x') = \pi^{-3/2} \int_{1/2|\tilde{x} - \underset{\sim}{x}|}^{\infty} e^{-u^2} \left[\tan^{-1}\left(\frac{\underset{\sim}{x} + u}{a}\right) - \tan^{-1}\left(\frac{\tilde{x} - u}{a}\right) \right] du , \tag{17}$$

where $\tilde{x} = \max(x, x')$ and $\underset{\sim}{x} = \min(x, x')$. The $R_{\text{II-A}}(x, x')$ given in the equation above is the well-known type II-A redistribution function of Hummer (1962). It is the angle-averaged scalar redistribution function for isotropic scattering. In the PRD computations, we have directly evaluated $R_{\text{II-A}}(x, x')$ from the equation (17) numerically. It refers to the two-level atom case whose upper level is naturally broadened and lower level has zero width.

The boundary conditions employed are in general

$$\boldsymbol{U}(x, \mu, \tau = T) = \boldsymbol{U}_*(x, \mu, r = 1) = 0.5 \text{ at } \tau = T, \mu > 0 , \tag{18}$$

and

$$\boldsymbol{U}(x, -\mu, \tau = 0) = \boldsymbol{U}_F(x, -\mu, r = R) = 1 \text{ at } \tau = 0, \mu < 0 , \tag{19}$$

for most of the computations presented here. $\boldsymbol{U}_*(x, \mu, 1) = 0.5$ refers to the unpolarized diffuse radiation emitted by the central core and incident on the adjacent lower boundary of the spherical atmosphere. $\boldsymbol{U}_F(x, -\mu, r = R)$ refers to the free space diffuse radiation field incident on the outer boundary of the atmosphere. The usual planetary nebula type boundary condition is given by

$$\boldsymbol{U}(x, \mu, r = 1) = \boldsymbol{U}(x, -\mu, r = 1) \text{ at } \tau = T . \tag{20}$$

III. METHOD OF COMPUTATION

We have employed the Peraiah-Grant method for solving the spherical radiative transfer problem. Since the basic method is described in detail in Peraiah (1984), we shall not go in any detail into that aspect. First, we have to generalize all the steps of this finite difference technique to include the polarization state of the radiation. Since we employ a two-dimensional vector $(I_l I_r)^T$ to represent the specific intensity vector, the matrices appearing in the computational algorithm will now be having dimensions twice as much for the corresponding scalar line transfer problem. The method of extending the algorithm to include the anisotropic absorption and scattering in the continuum (e.g., transfer in a strongly magnetized plasma) is described in Nagendra and Peraiah (1985) with applications. The true absorption Zeeman line transfer problems are treated in Nagendra and Peraiah (1987) and Nagendra (1987).

Basically the spherical medium is divided into a number of spherical layers. The transmission ($\boldsymbol{T}$), reflection ($\boldsymbol{R}$) and source vector ($\boldsymbol{\Sigma}$) are computed for all the layers. $\boldsymbol{R}$, $\boldsymbol{T}$, and $\boldsymbol{\Sigma}$ operators for thick layers can be generated using the so-called star product (starting with the operators for the fundamental "cell"), which is essentially a doubling algorithm. The method is unconditionally stable and provides accurate solutions as long as the conventional normalization conditions on the polarized redistribution matrix plus the step-size criterion for the spherical fundamental "cell" are satisfied. In practice, these conditions can be easily satisfied if we work with reasonably good resolution in frequency quadrature, angular quadrature, and spatial discretization. Along with the self-

consistancy check on the solution (e.g., global flux conservation in a conservative scattering medium: $\epsilon = \beta = 0$, etc.), we have compared the CS, CRD, and PRD intensity and polarization profiles with the corresponding profiles in PP medium, kindly provided by Rees and Saliba. The results computed by them using the Feautrier scheme, and our results match up to third or fourth digit after the decimal even for a very modest choice of 13 or 15 equally spaced trapezoidal frequency points. A comparison for PRD profiles is also made with the published results of Faurobert (1987). The spherical transfer results are compared with some test cases of Mihalas, Kunasz, and Hummer (1975). Once the diffuse radiation field has been computed at all the shell boundaries of the SS or PP medium, the moments of the specific intensity as well as the source function are easily computed. These spherically symmetric source functions are useful in a separate computation where the intensity and polarization profiles are now computed in the line of sight. This calculation is quite simple and employs the formal solution of the transfer equation along the rays parallel to the line of sight and drawn tangential to the shell boundaries. Such a calculation provides the distribution over the stellar disk, of the specific intensity vector $\boldsymbol{I}(x, h)$ as a function of the impact parameter h—the perpendicular distance of the ray from the center of symmetry. We also get emergent flux profiles from the line of sight program. Note, however, that the disk-integrated linear polarization in the SS model is identically zero.

a) Model Parametrization

The models employed are highly idealized and aimed at understanding the basic features of the polarized line formation problem in spherical systems. The spherically symmetric models are characterized by spherical shells of outer radius R and optical thickness T surrounding a central core of radius $R_C = 1$, which is the unit of length for all the shell models. Except mentioned otherwise, the central core is always taken to emit an isotropic radiation of intensity 1, so that $\boldsymbol{U}(x, \mu, T) = 0.5$. This is called the Schuster boundary condition, which is a stellar atmospheric-type boundary condition. For isothermal models, the optically thick Schuster boundary condition is equivalent to the diffusion approximation boundary condition (see Mihalas, Kunasz, and Hummer 1975). The PP limit is recovered by putting $R \equiv 1$ in the computations. $R \neq 1$ refers to SS media. Following suggestions by Kunasz and Hummer (1974), we have everywhere used an inverse square opacity law unless otherwise stated. In terms of R and the total line optical thickness T,

$$k^L(r) = Kr^{-2}, \qquad K = RT/(R-1), \tag{21}$$

and the optical depths are given by

$$\tau^L(r) = \frac{RT}{(R-1)}\left(\frac{1}{r} - \frac{1}{R}\right). \tag{22}$$

The continuum thermalization parameter β is chosen so as to represent a thick continuum which is generally found in stellar atmospheres. The total optical depth in the continuum is $T^C = \beta T$. The radial distribution of continuum opacity and optical depth are given by $k^C(r) = \beta k^L(r)$ and $\tau^C(r) = \beta \tau^L(r)$, respectively. The contribution to continuum emission could be from not only the atomic continuum absorption, but also from any other physical mechanisms such as electron or dust scattering. The values of β selected in this paper correspond to large values of T^C and are in conformity with the Schuster boundary condition employed in the computations, through the presence of a thick continuum at all the frequency points in the line.

The values of the line thermalization parameter ϵ are taken in such a way that atmosphere is few thermalization units ($\sim \epsilon T$) thick. It is well known (see Kunasz and Hummer 1974) that the atmospheric extension effectively reduces the actual thermalization thickness for a given value of ϵ.

The Planck function which acts as the continuum thermal source of radiation in the atmosphere has been chosen to be $B'(r) = 1$ unless mentioned otherwise. It represents an isothermal atmosphere with a photon creation rate per unit optical depth proportional to r^2.

We have assumed a Voigt line profile in all the cases. The frequency band width is chosen so that the line opacity at the last frequency point in the wing $\tau_x = T\phi(x)$ is much less than the continuum optical depth T^C. The number of trapezoidal frequency points is 13 or 15 with a spacing $\Delta x \leq 0.5$. Integrations over μ are performed with a three-point Gaussian quadrature formula on the interval $0 < \mu < 1$. The number of spatial points in the radial grid depends on the value of R. Generally 30 to 40 equally spaced (or logarithmically spaced) radial points are enough for small extensions ($R < 10$) of the atmosphere. Angle points: $\mu_1 \approx 0.11$; $\mu_2 \approx 0.5$; $\mu_3 \approx 0.89$.

b) Computing Time

The dimensions of the matrices appearing in the computing algorithm are (NT, NT), where NT = NP × NF × NA, where NP is the number of polarization states, NF is the number of frequency points, and NA is the number of angles. The computing time scales roughly as cube of the quantity $(NT)^2$. Also, since the "fundamental cell" operators have to be computed for each of the spherical shells in view of the varying curvature factor over the atmosphere (even in a constant property media), the computing time linearly scales as the number of depth points. The treatment of high optical depths is not much of a problem since the thick shell reflection, transmission, and internal source operators can be generated by a fast and accurate doubling algorithm as already mentioned. The disk-integrated (line of sight) flux profiles can be computed in a separate program which is simple, since it employs the formal solution along the parallel rays using the already computed spherically symmetric source functions.

IV. RESULTS AND DISCUSSION

a) Effect of Sphericity (R) on the Intensity and Polarization Profiles

Here we discuss the sphericity (or curvature) effects using weakly or moderately extended spherical shell like atmospheres. The solutions are compared with analogous PP models. In Figure 1, we show the effects of sphericity. The full lines are the emergent intensity profiles log I referred to the scale on the right-hand side of the figure. The dashed lines are emergent linear polarization profiles $(Q/I)\%$ referred to the scale on the left-hand side. The quantities x are the reduced frequency points in the line. Unless stated otherwise, the intensity and polarization profiles are always shown for the direction $\mu_1 \approx 0.11$. This convention is followed in most of the figures given in this paper. The model parameters T, a, ϵ, and β are given in all the figures in a similar way. The curves labeled $R = 1$ correspond to the PP slab model. The atmosphere is moderately and effectively thick ($\epsilon T > 1$); i.e., the escape probability is low, at least in the PP limit. CRD is the redistribution function used in the calculation. The $R = 1$ intensity profile is a pure absorption line. The polarization has the expected behavior of negative core maxima, and a very small positive polarization peak around $x \approx 2$. Because of the dominance of the unpolarized continuum opacity, the polarization is slowly driven to zero in the near wing $x \approx 4$ itself. The curves with $R = 3$, $k(r) = K$, and $B'(r) = 1$ refer to the profiles formed in a constant opacity isothermal spherical atmospheres, with an emitting core. Notice that $K = T/(R - 1)$ in a constant opacity model. The specific intensity of the SS solution is much smaller than in the PP limit. This is so because of the characteristics of the spherical radiative transfer. The first characteristic is the "bias" in scattering toward the larger radius—namely the photon scattered from a certain radius ends its flight at a larger radius more often than at the smaller one. On the other hand, in PP geometry, a photon goes with equal probability to larger or smaller depths. As shown in Kunasz and Hummer (1974), the bias is most important in the inner regions. It is seen from the figure that the effects of spherical geometry do not develop fully in the rather special case of constant opacity atmosphere. It is seen that there is not much difference between the shape of the PP and SS intensity profiles. The second characteristic of the spherical

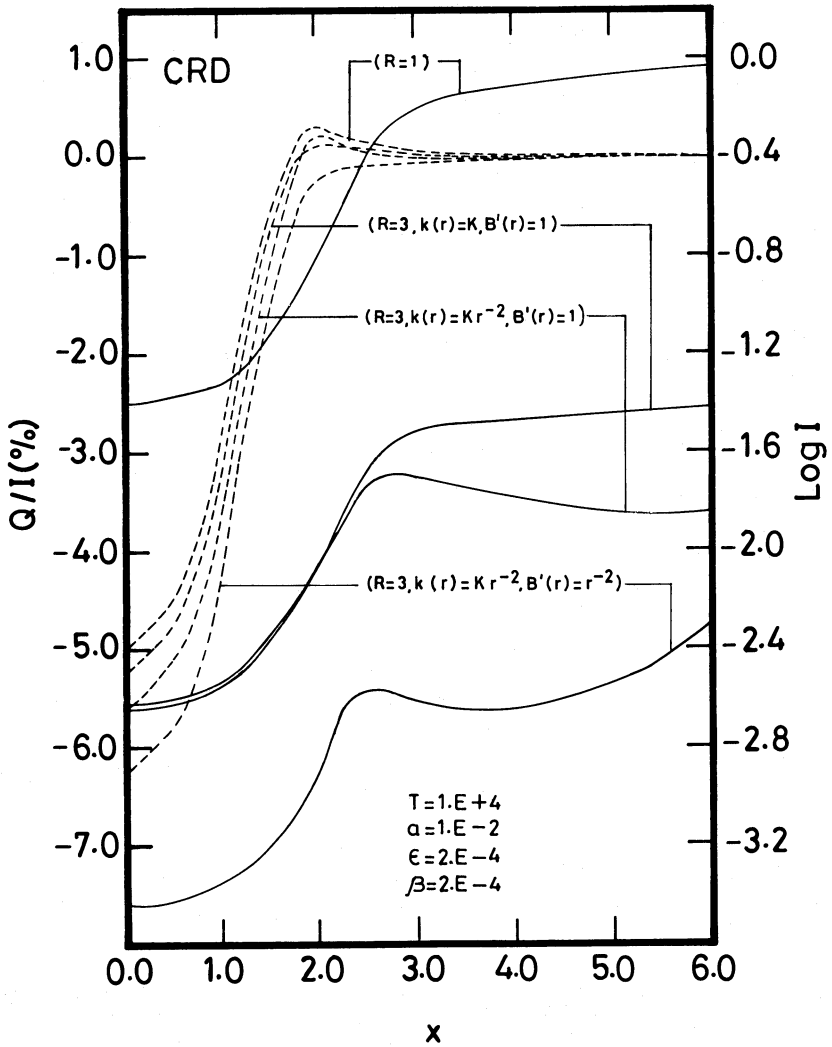

FIG. 1.—Emergent intensities I (*solid lines*) and polarizations Q/I (*dashed lines*) in the direction $\mu_1 = 0.11$ in plane-parallel ($R = 1$) and spherically symmetric ($R \neq 1$) configurations for the given model (T, a, ϵ, β) and the parameters shown near the lines. Symbols are described in the text.

geometry is the "dilution" of diffuse radiation field. This dilution factor is given by $2W = J(r = R)/J(r = 1) = [1 - (1 - 1/R^2)^{1/2}]$. It is clearly seen that there is a rapid decrease in W for values of R even slightly exceeding unity, and it gradually saturates for large values of R. Hence even small departures from planar limit produce significant weakening of the mean intensity J. The third characteristic of the spherical transfer is the "peaking" of the radiation in the radial direction for extended spherical systems. This is due to the fact that a ray emitted in any direction at a deeper point in the atmosphere and traveling in the outward direction obviously makes smaller and smaller angles with the radii drawn at the intersection points of this ray with the subsequently occurring outer shell boundaries. This is sometimes called curvature scattering. This final characteristic causes numerical difficulties in treating highly extended systems, through the need to take large number of angular points. The characteristics mentioned above are common for all the results on spherical systems that are presented in this paper. It is also important to note that the difference between the PP and SS solutions is minimum for $\mu \to 1$.

The curves labeled [$R = 3$; $k(r) = Kr^{-2}$; $B'(r) = 1$] represent the SS solution for inverse square opacity law (see eqs. [21] and [22]). For this choice, the bias is particularly important and largest in the outer regions, because the photon mean free paths in the outward direction can be substantially longer than in the inward direction. For this reason the estimates of the intensity and polarization computed with escape probability methods become less reliable than for PP systems.

For the inverse square opacity variation, the effects of sphericity clearly manifest themselves. The important difference between PP and SS situations is that there is a small emission in the near wings ($x \sim 3$). The magnitude of the emergent radiation in the far wings is small because most of the thermal photons that are created near the stellar core cannot easily escape because of the high optical depth in the wing in the layers near the stellar core. The degree of polarization in the line core is larger than the PP case. In the wings its behavior is similar to that of PP and $k(r) = K$ case, although its peak value is slightly higher than the $k(r) = K$ case. The curves labeled $R = 3$, $k(r) = Kr^{-2}$, and $B'(r) = r^{-2}$ represent a case, where the photon creation rate per unit optical depth is constant, as it is for isothermal PP case. In this case, the thermal contribution $\epsilon B'(r)\mathbf{1}$ to the total source function $\boldsymbol{S}(r)$ is small almost throughout the atmosphere excepting in deep layers. This results in the depletion of unpolarized thermal photons in the outer layers leading to an increased degree of anisotropy in the local diffuse radiation field. Hence the degree of polarization of the emergent line profile is also large and always negative. The "dilution effect" is accentuated here than the $B'(r) = 1$ case, since in the latter case, the increased photon creation rate toward the surface disguises the dilution effect. The intensity profile has a near wing emission here also. The line radiation field itself has a dominant role throughout the line profile. It should be noted that the emission peaks in the intensity profiles do not correspond to the positive polarization peaks in the polarization profiles. The latter are shifted toward the line core.

b) *Effect of Thermalization Parameter* ϵ

The effect of ϵ on the polarization profiles in PP slabs has been discussed in Dumont *et al.* (1977). In Figure 2, we have compared the line profiles computed in the PP limit and the SS model with $R = 3$ and $B'(r) = r^{-2}$. The ϵ values are selected in such a way as to represent effectively thick ($\epsilon T = 200$), effectively moderately thick ($\epsilon T = 2$), and effectively thin ($\epsilon T = 2 \times 10^{-2}$) lines. As ϵ decreases, scattering becomes more important, and, as expected, the degree of polarization increases in PP as well as SS models. The polarization is fully negative for $\epsilon = 2 \times 10^{-6}$. It has a small positive polarization peak for $\epsilon = 2 \times 10^{-4}$, and the behavior of double peak is further strengthened for $\epsilon = 2 \times 10^{-2}$. There is also a systematic shift toward line center as one goes from strongly scattering (small ϵ) to the weakly scattering (large ϵ) media. It is thus clear that the emergent polarization in the line profiles is a sensitive function of the thermalization parameter ϵ. As the ϵ value decreases, the spectral lines are more and more saturated, with a deepening of the core and a smaller change in the continuum level in the far wings. Since ϵ is proportional to the electron density, ϵ has a diagnostic potential in the interpretation of stellar line polarizations. From this figure it is also clear that the spherical extension will not essentially modify the saturation properties of the medium. Surprisingly the difference in the polarization profiles between $R = 1$ and $R = 3$ is quite large for a large value of ϵ wherein, the importance of line scattering being relatively small, the difference in these two cases should have been smaller than the $\epsilon = 2 \times 10^{-6}$ and 2×10^{-4} cases (see Kunasz and Hummer 1974). When $\epsilon = 2 \times 10^{-2}$ thermalization of the line radiation is strong, and the escape of line photons from the deep layers to the outer layers is more difficult. Since the radiation emerging in the line core is clearly dominated by contribution from the outermost layers (which have obviously higher degree of negative polarization), the degree of polarization is quite large compared to the PP case. Figure 3 shows the ϵ effect in an isothermal spherical atmosphere with $B'(r) = 1$. As compared to the $B'(r) = r^{-2}$ results of Figure 2, here the LTE situation $\epsilon = 1$ (for which the polarization is identically zero) as well as the pure scattering in the line $\epsilon = 0$ case are also shown. The discussion given above for Figure 2 holds here also qualitatively. It can be seen that an absorption line gradually becomes an emission line as one goes from $\epsilon = 0$ to $\epsilon = 1$ in a SS model. In the SS model, the line cores are mainly formed in outermost layers. Thus the core region of the line has a larger effective emitting area. Thus, in this LTE isothermal SS model the line will appear in emission relative to the continuum. This is in contrast with the isothermal PP model in LTE, where the line is neither in emission nor absorption.

c) *Effect of Optical Depth* T *in a Spherical Atmosphere*

The frequency integrated line optical depth T is an important parameter of the problem. The SS intensity and polarization profiles for three values of T are shown in Figure 4. $T = 2500$ corresponds to a moderately optically thick $(aT)^{1/3} \sim 1$ and effectively thin $\epsilon T \ll 1$ line, while the other two values of T correspond to optically thick and optically very thick lines. There is a thick continuum in this model which is also taken to be highly scattering. The high value of a also implies a stronger non–LTE situation in the model. Because of such a combination of parameters, the intensity profiles are highly saturated. Higher values of T produce a change only in the intensity of line wings. $T = 2.5 \times 10^4$ and $T = 10^6$ intensity profiles are indistinguishable in the line core and not much different in the wings either. It is clear that the increase in multiple scattering with an increase in T causes a "reduction" in the negative polarization in the line core. The multiple scattering appears to enhance the positive polarization all

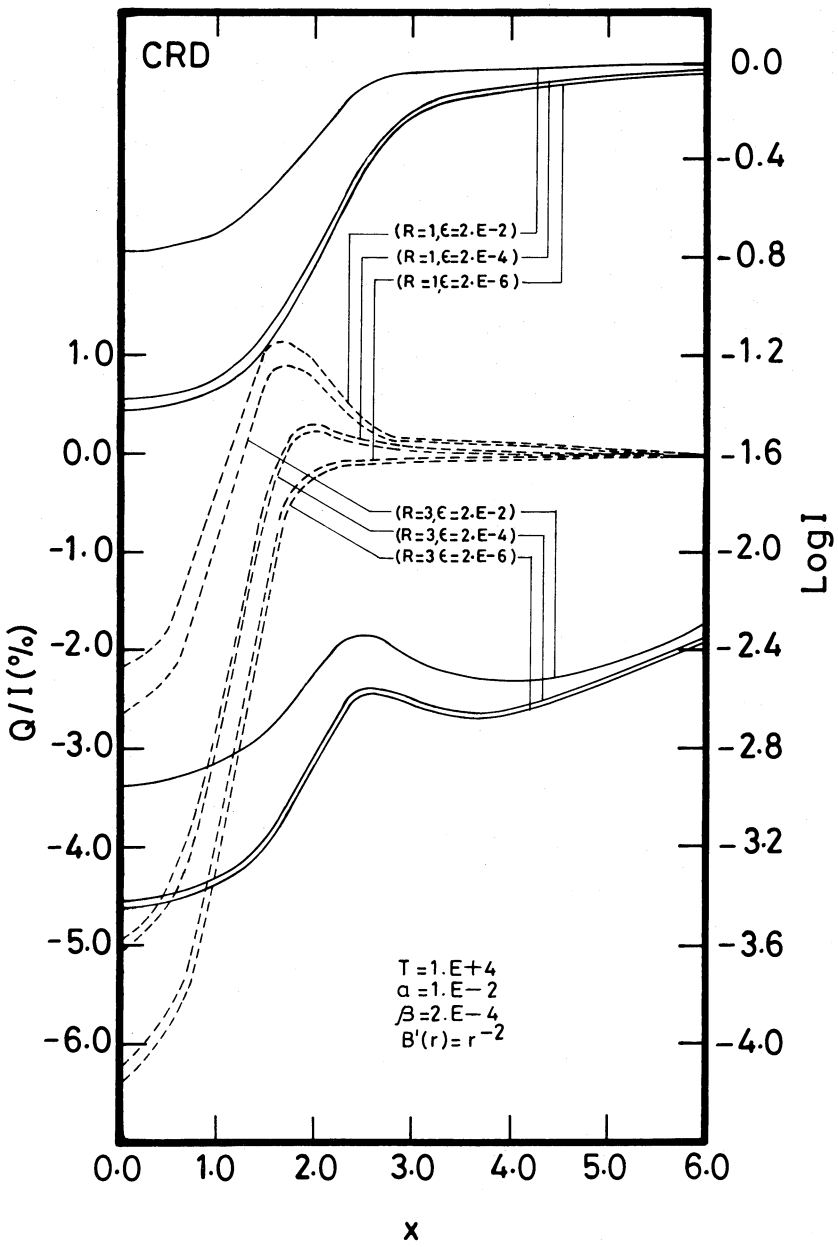

FIG. 2.—Effect of thermalization parameter ϵ. Values of ϵ are given near the lines. The inverse square variation of the Planck function $B'(r)$ is used in the computation of these results. See Fig. 1 also.

over the line, although continuum radiation is strong enough to mask such effects in the line wing and thus lead to the expected gradual convergence of polarization to zero. The enhancement of the positive polarization peak near the Doppler core is similar to the effect of ϵ parameter shown in previous § IV*b*. The reason is that increasing the value of T is in a way equivalent to increasing the value of ϵ. It is informative to compare the optical depth effects in the line profiles (for $T = 1$–100) shown in Rees and Saliba (1982) and Faurobert (1987) and those presented here (for the lines which are optically thick in general). The polarization profile in particular is a very sensitive function of T and ϵ and its behavior in emission lines formed in spherical atmospheres cannot be understood by extrapolation of the present results. And hence separate calculations have to be done for the models producing emission lines. This is not to speak of lines with $T < 1$ which have their own special behavior as far as polarization is concerned, arising due to the dominance of single scattering. We also note that in general the intensity and polarization profiles are not very sensitive to the finite values of β parameter in optically and effectively thick lines. In addition, for the high values of β used by us, the continuum optical depths are large for all the values of T used in Figure 4. The continuum radiation field, being in LTE, is spatially localized. Such a large thermal source of photons is coherently scattered in the line wing, the amount of scattering being proportional to the value of T.

In the presence of a thick continuum, the increase in T results in a small deepening of the I profile at the center, due to the increased coupling of the core to the wings and the wing depression seen in the $T = 2500$ case is filled up. For the same reason, the

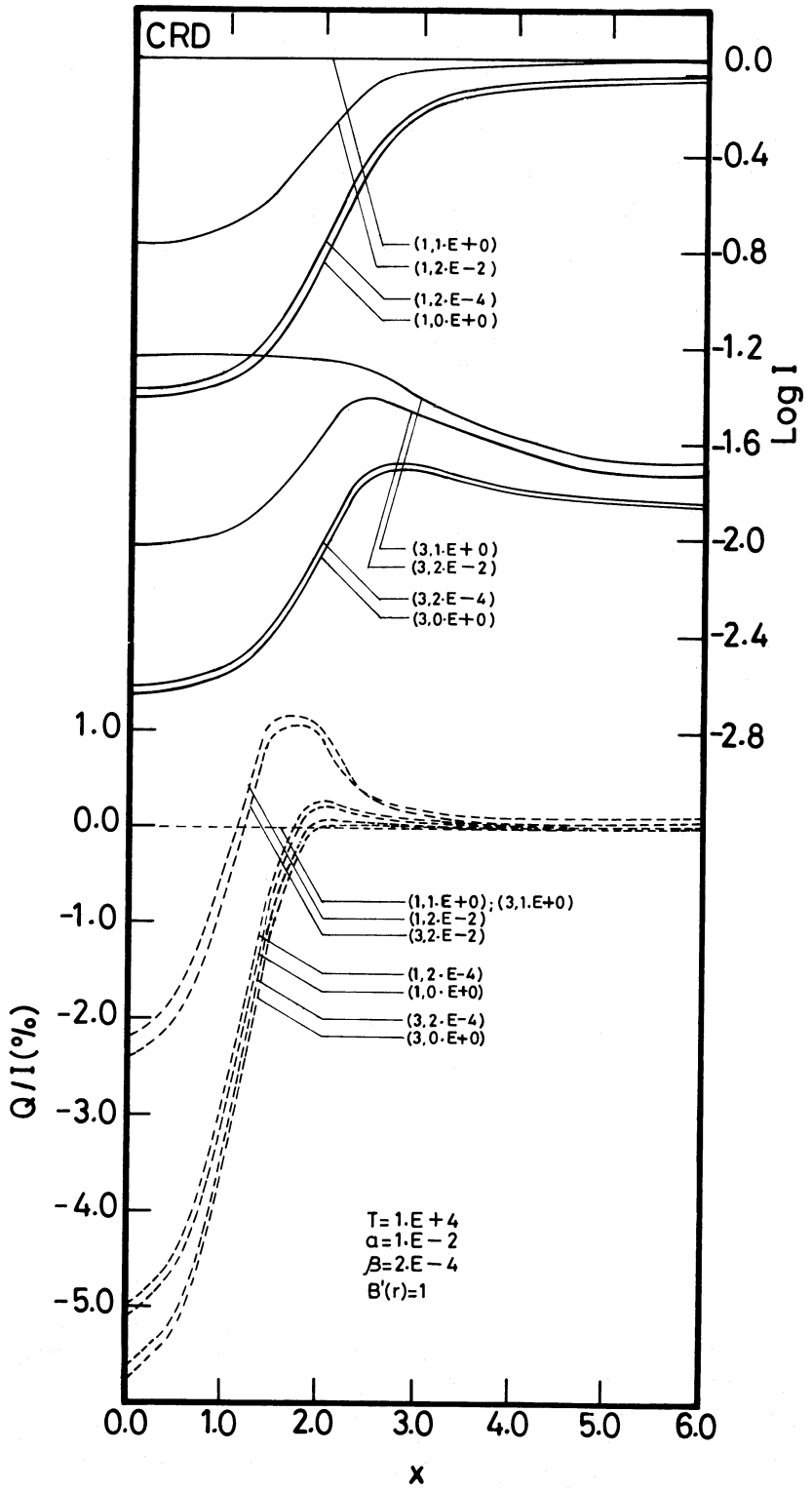

FIG. 3.—Same as Fig. 2, but for the constant value of the Planck function $B'(r) = 1$ in the atmosphere

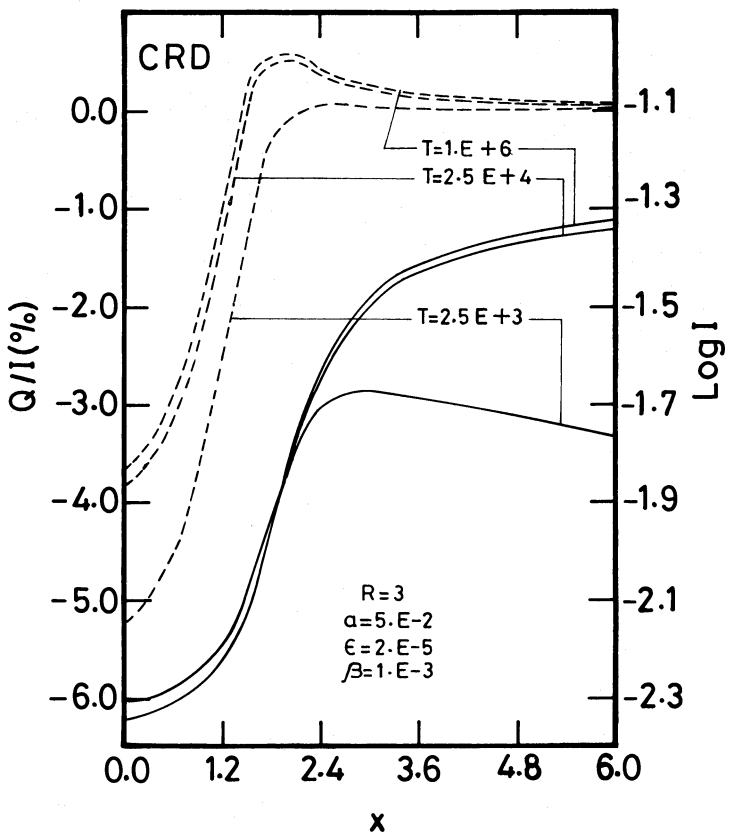

FIG. 4.—Effect of optical depth T. Note that a different model is used here. Inverse square opacity and constant Planck function values are employed.

polarization in the wings also increases slightly and the approach to zero is more gradual. As T increases, the amount of positive polarization (the polarization parallel to the surface) increases over the full bandwidth of the line.

d) Effects of the Boundary Conditions in a Spherical Atmosphere

Figure 5 shows the profiles corresponding to some of the familiar boundary conditions used in the spherical radiative transfer work. The "emitting core" refers to the boundary condition we have employed throughout this work [$U_*(x, \mu, r = 1) = 0.5$]. It is clearly a stellar atmosphere boundary condition. The "hollow core" means the absence of the central core in a spherical envelope. It is also called the planetary nebula boundary condition and is widely used (see eq. [20]). The "black core" refers to a truly absorbing core. It is also called black hole boundary condition, since the core does not emit either [$U_*(x, \mu, r = 1) = 0$]. The I profiles and hence the polarization profiles are quite insensitive to these three types of boundary condition in the present models, the reason being the high values of optical depth and the effectively thick regime in the optical depths, which closely resembles the photospheric conditions. The line core which is formed mainly in the outermost layers is hardly affected. Since the wing photons come mainly from the deeper layers, the changes in the lower boundary condition can cause a smaller or larger change in the line wings depending on the total optical depth T and the value of β through the importance of continuous absorption. The "black core" intensity profile has a depressed wing obviously because the back scattered diffuse radiation field toward the central core is totally absorbed, causing a depletion of the wing photons. The emitting, hollow and black core in order, cause increasingly higher degree of anisotropy in the radiation field at the region of the central core of the model atmosphere. See Mihalas, Kunasz, and Hummer (1975) for further details on these boundary conditions. When the hollow core model is illuminated on the outer surface by a strong diffuse radiation field $U_F(x, -\mu, r = R) = 0.5$ the source function gradient (over the optical depth scale) that is set up in the conventional zero illumination case is highly smoothed. In the same manner the source function $S(x, \mu, r)$ becomes almost depth independent. Because of the dominance of imposed isotropic radiation field in the outermost layers, where polarization actually arises, the degree of polarization of the emergent line profile is extremely small. The I profile is in emission since the photon density in the surface layers where line core is formed, is high, due to the illumination.

e) A Comparative Study of Lines Formed under CRD, PRD, and CS Mechanisms

The resonance line PRD transfer problem is a highly explored topic. The polarization transfer calculation taking PRD effects into account through the $R_{II\text{-}A}(x, x')$ function is also well known (e.g., Rees and Saliba 1982; Faurobert 1987, 1988). In the Figures 6–7 and 10–11 we have shown the PRD source functions and line profiles as compared to the corresponding quantities in CRD. The CS source functions (Figs. 8–9) and line profiles (Fig. 12) are shown separately. The PP and SS models are also compared to help understand the role of PRD in SS solutions. The figures are self-explanatory and can be easily understood based on the existing

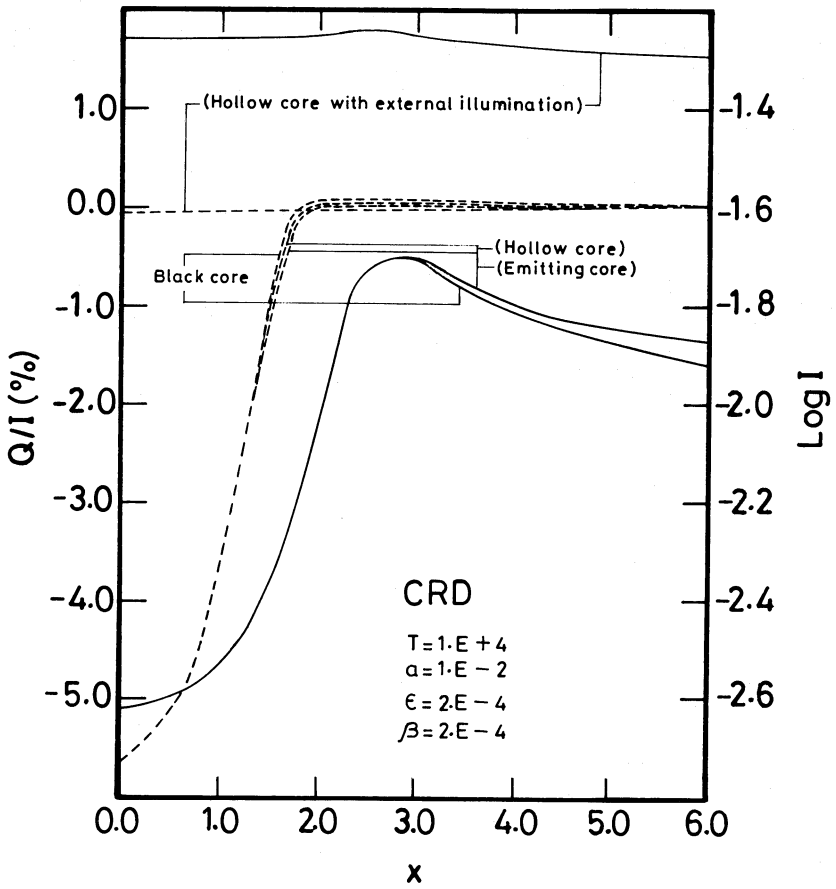

FIG. 5.—Effect of boundary conditions on the intensity and polarization profiles. See the text for the boundary conditions.

literature on the scalar PRD resonance line transfer solutions and the investigations mentioned just above. In general, the PRD line profiles behave like CRD profiles in the line core and like CS profiles in the far wings. This is due to the strong wing coherence exhibited by the $R_{\text{II-A}}(x, x')$ redistribution function. Because of rather large continuum opacity ($\beta = 2 \times 10^{-4}$) used by us, the PRD effects in intensity and polarization profiles are not fully revealed in the PRD results. In fact, the region $x \lesssim 3$ is the only frequency region in the near wings where we have allowed PRD to play its role, since regions with larger x, where the effects of PRD would be actually greater, are more and more dominated by the continuum. The conditions for the importance of line scattering represented by PRD mechanism, in the presence of a continuous absorption in the wings of resonance and subordinate lines have been investigated by Hubený (1985). The inequality $\beta \ll a/\pi^2$ represents this condition for the importance of PRD effects. For our present choice of parameters ($\beta = 2 \times 10^{-4}$; $a = 10^{-2}$), this inequality is only marginally satisfied ($2 \times 10^{-4} \lesssim 10^{-3}$).

Figure 6 shows the optical depth dependence of the intensity source function S_I, at three frequency points in the line. The amount of scattering is more in PRD at any x, as compared to the CRD. This can be seen by comparing the values of respective redistribution functions. In the PP case, the difference between CRD/PRD source functions is the largest in the outermost layers of the slab model. This is in contrast with the results for optically thin nonilluminated self-emitting slab wherein the CRD/PRD source functions differ mainly in the deeper layers of the slab model. The difference between CRD/PRD source functions is significant only in the outer layers, where line core is formed. The difference between the CRD/PRD source functions vanishes deep in the atmosphere ($\log \tau \approx 3.5$), for all the frequency points $x = 0$, 3, and 6. The results for the SS model are computed taking a fairly extended atmosphere ($R = 10$). Notice that the SS model source function dependence on optical depth is qualitatively similar to the PP model, throughout the atmosphere. The convergence of S_I for all the frequency points takes place at a comparatively smaller depth ($\log \tau \sim 3$). Figure 7 shows the optical depth dependence of the S_Q for CRD/PRD cases in the PP and SS models. The main feature is the vanishing of linear polarization in the deepest layers ($\log \tau > 4$) due to extreme thermalization of the radiation field which becomes isotropic in nature. The CRD source functions S_Q for $R = 10$ are very small throughout the atmosphere in the adopted scale. Notice, however, that S_I is in log scale and S_Q in linear scale. For the emergent polarization, it is the ratio S_Q/S_I is what matters, not S_Q itself. This ratio represents the polarization content of the radiation field at any point in the atmosphere. Clearly, the mean intensity and source function are much less in the outer layers of a spherical system as compared to the PP case, because of the dilution effect in the former. A characteristic variation of PRD source functions S_Q for $R = 1$ is clearly seen. This variation is strongly reflected in the emergent polarization profiles, and naturally explains the existence of larger positive polarization in the far wings $x = 6$, in most of the PP models. It is clearly seen that the SS model smoothens the strong depth dependence seen for $R = 1$, of PRD source function of S_Q; also S_Q is not positive in the deepest layers. However, the smooth oscillations of these

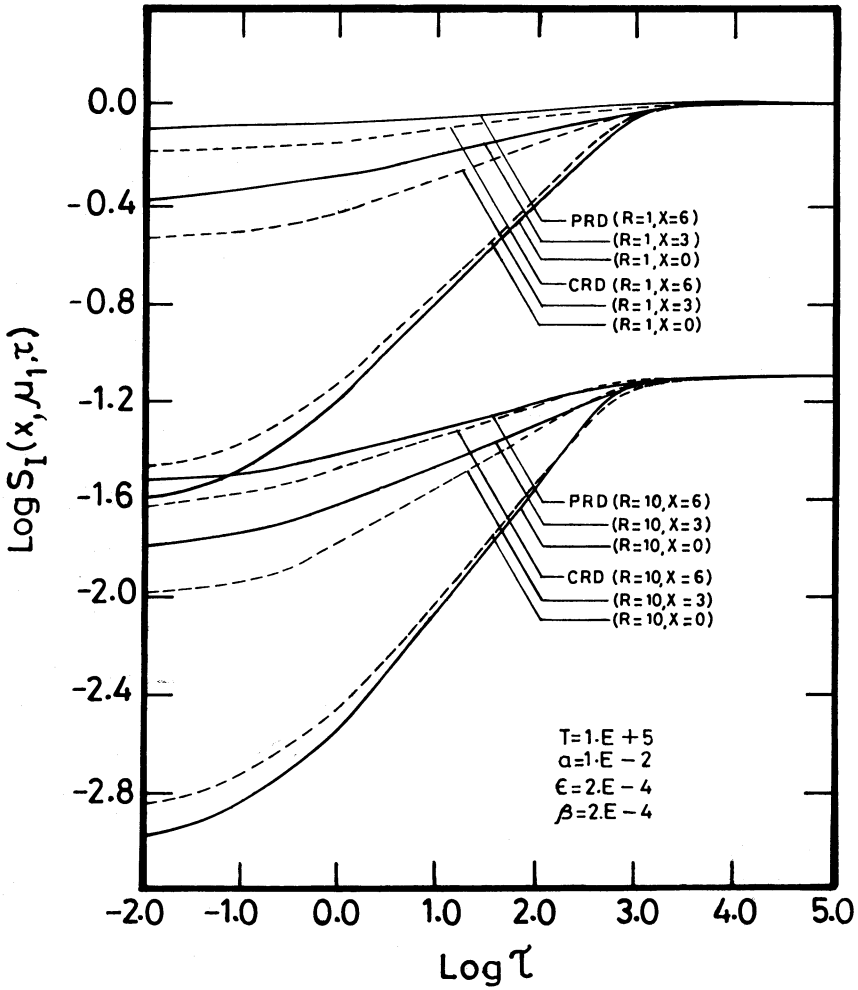

FIG. 6

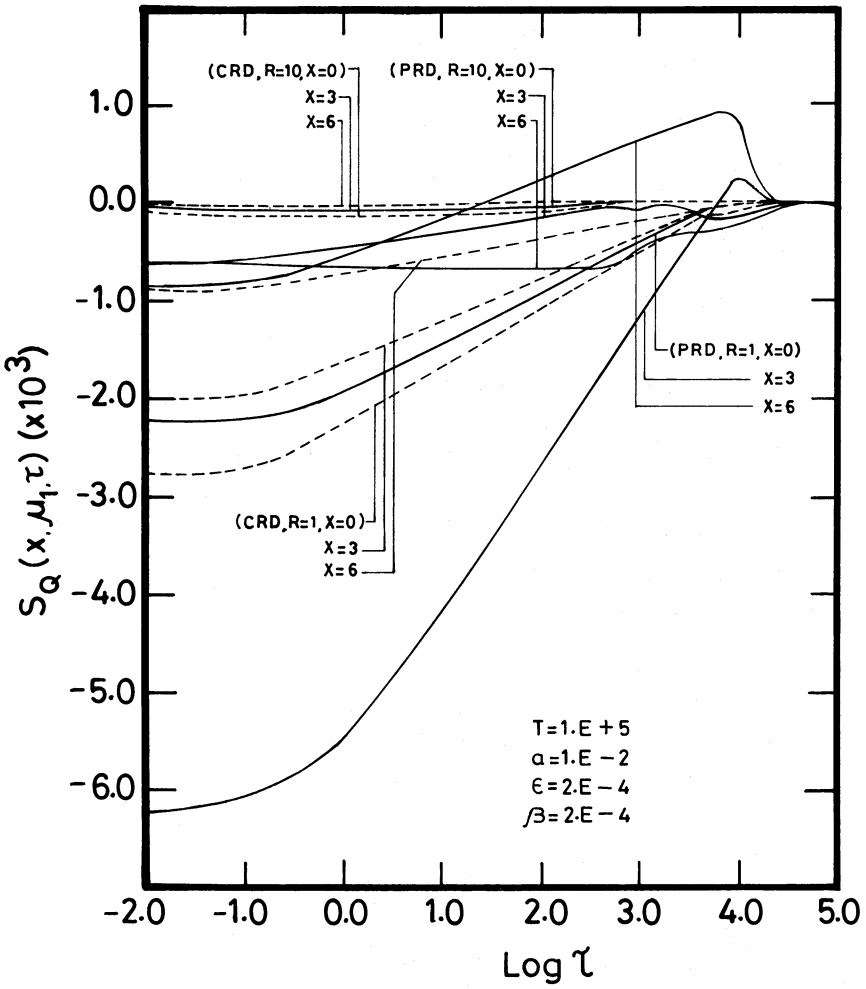

FIG. 7

FIG. 6.—CRD vs. PRD comparison on the depth dependence of the intensity source function S_I for the angle $\mu_1 = 0.11$. *Solid lines*, PRD; *dashed lines*, CRD.
FIG. 7.—Same as Fig. 6, but for the polarized source function S_Q

S_Q source functions in the deepest layers of $R = 10$ model are responsible for the wing behavior of the corresponding polarization profiles in Figure 11.

The coherent scattering in a two-level atom is an idealistic situation. It has been studied to get an estimate of the maximum amount of polarization obtainable in a given model. A detailed study of CS line formation in semi-infinite atmospheres has been done by Rees and Saliba (1982). We now indicate characteristics of this problem in finite atmospheres. Figure 8 shows the depth dependence of S_I for three frequency points in the line. It can be seen that variation of S_I with τ is generally similar to that of CRD and PRD mechanisms, and the impact of sphericity is also as expected. A comparison of this figure with Figure 6 shows that values of S_I for CS are substantially larger than the S_I of CRD/PRD at all frequency points. This observation is true through major part of the line-forming region excepting the outermost part of the atmosphere. This characteristic is stronger in the SS model than in the PP model. Deep in the atmosphere ($\log \tau \gtrsim 3$) the details of the depth dependence in CS source function S_I are more pronounced than in the CRD/PRD source functions, although PRD and CS source functions are particularly similar in their depth dependence. Figure 9 shows the depth dependence of the polarized source function S_Q. Once again, like PRD, there is a sharp rise of the line wing ($x = 3$ and $x = 6$) S_Q source functions in the deepest layers of PP model. This is due to a larger number of scatterings in the line wing which is actually formed in these very layers and, moreover, due to the lack of frequency coupling to the inner parts of the line profile. Thus the line center ($x = 0$) polarized source function S_Q has small values in the deepest layers and varies also smoothly without changing sign. It is interesting to note that S_Q in the SS model have small negative values and after an initial increase, almost remain constant throughout the atmosphere. Thus, in a coherently scattering medium, the sphericity appears to increase the negative polarization content throughout the line profile. It may be due to the usual spherical radiative transfer effects which are discussed earlier.

In Figure 10 we have shown the emergent intensity and polarization profiles for CRD mechanism in the PP and SS models. We have included the angle dependence of emergent profiles also. The CRD profiles are already discussed in the previous sections, and we do not repeat it here. The medium is optically and effectively thick ($T = 10^5$; $\epsilon T = 20$; $[aT]^{1/3} = 10$) with a strong continuum emission. The emitting core boundary condition is taken. The opacity $k(r) = Kr^{-2}$, and Planck function is $B'(r) = 1$. The PP and SS solutions have similar behavior, except for a slightly higher degree of polarization in the SS case. The usual intensity limb darkening

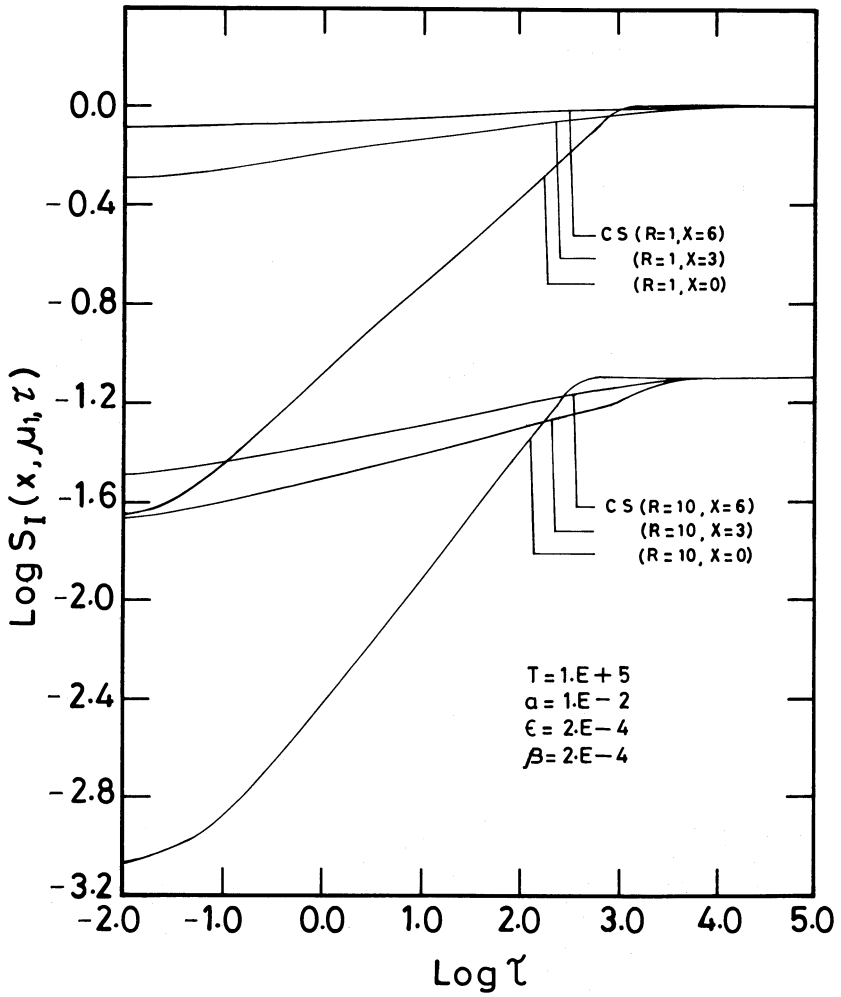

FIG. 8.—Depth dependence of the CS intensity source function S_I for the direction $\mu_1 = 0.11$

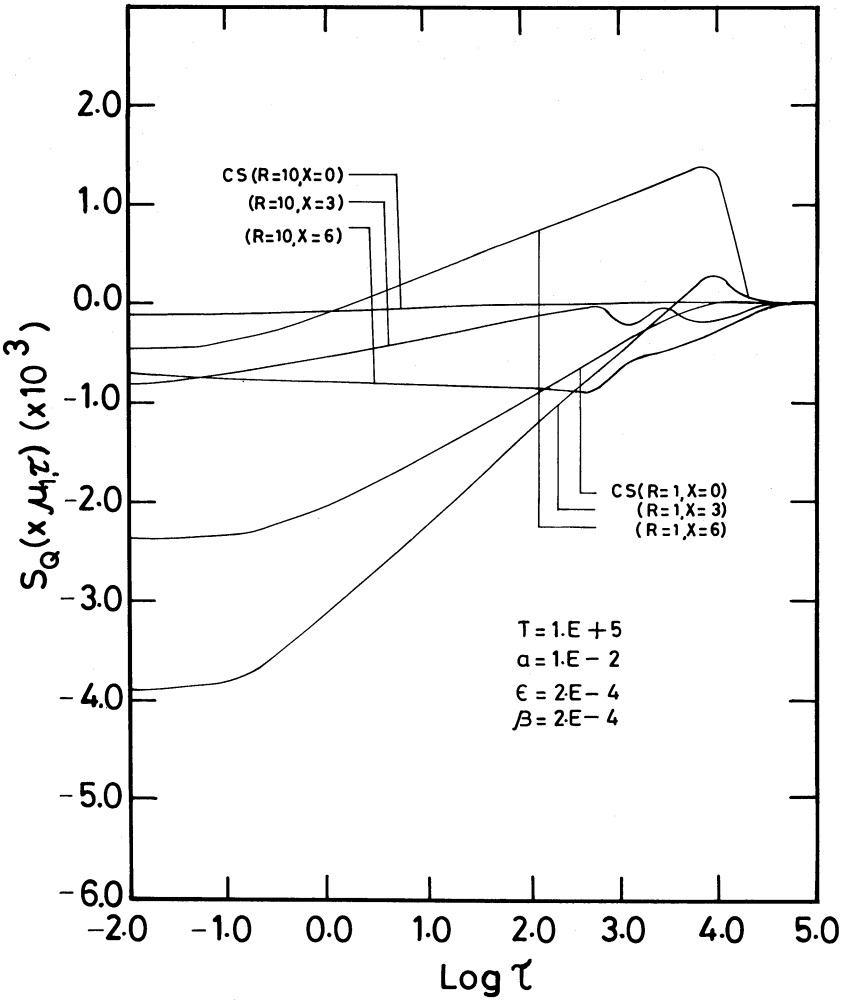

FIG. 9.—Same as Fig. 8, but for the polarized source function S_Q

and the decrease of polarization toward the symmetry axis (Z-axis of slab or the radius r of SS model) is evident. In Figure 11 the corresponding PRD situation is shown. A comparison CRD versus PRD shows that the I profiles are deeper at the line center and differ subsequently in the line shape up to $x \sim 3$ in the PRD case. In the far wings, the difference is negligible. This comparison is again in contrast with the optically thin profiles (e.g., Faurobert 1987, Rees and Saliba 1982). The polarization profiles are, however, quite different for CRD and PRD cases. The behavior in the inner core of the line is similar in these two cases. The CRD polarization profiles, however, rise from negative maxima quite rapidly and reach almost zero value in the near-wing region itself, after a small positive peak. The PRD polarization profiles, on the other hand, rise slowly and reach a positive maxima around $x \sim 3.5$ and slowly decrease toward zero value in the far wing. The PRD polarization profile is wider than the CRD polarization profile. The wing polarization is always positive in the PP situation. In the SS case the polarization behavior is more interesting. There appears to be two negative polarization maxima, one at the line center and the other somewhere in the far wing: $x \sim 5$. The sign of polarization is always negative throughout the PRD line profile. This behavior can be understood through the S_Q/S_I behavior over the optical depth, deep in the atmosphere. The reason for this kind of wing behavior in PRD polarization is the wing coherence, which means that the behavior of PRD function is more similar to the CS redistribution function in the far wings. The PRD function has, however, the additional property of introducing frequency diffusive nature into the line profile directed from far wing toward the line center. The positive maxima in PP and far-wing negative maxima in SS are due to the importance of polarization preserving CS contribution which also retains the polarized photons at the line wing frequencies itself during the scattering process.

In the Figure 12 we have shown the emergent intensity and polarization profiles for CS. The CS intensity profiles in both PP and SS are slightly broader than the PRD and CRD profiles. The CS intensity I profiles for μ_1 are deeper than PRD profiles at $x = 0$. But, for other two angles μ_2 and μ_3, the PRD intensity profiles are deeper than the CS profiles at the line center. The CS intensity profiles are deeper than the CRD profiles throughout the bandwidth and for all angles. Basically CS is a mechanism which generates a higher degree of linear polarization as compared to CRD/PRD. A comparison of Figures 12 and 11 shows that, although the shapes of the polarization profiles in PRD and CS look similar for all the angles $\mu_{1,2,3}$, the positions of the peaks are significantly different. Because of the CRD–type nature of PRD in the line core, the PRD polarization profile also is narrow just as CRD,

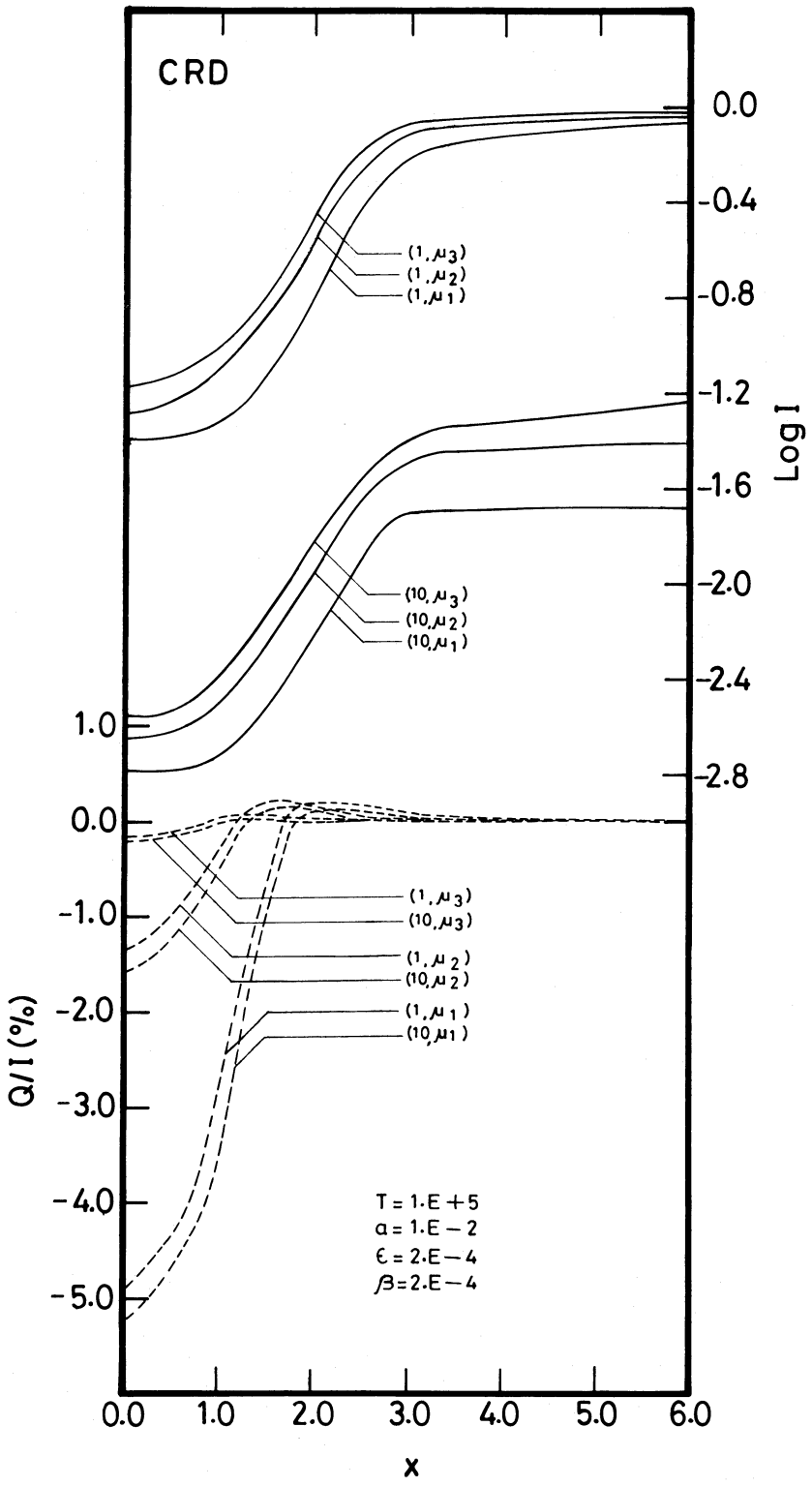

FIG. 10.—Angular dependence of the emergent I and Q/I profiles corresponding to the model of Figs. 6 and 7. The line scattering mechanism is CRD.

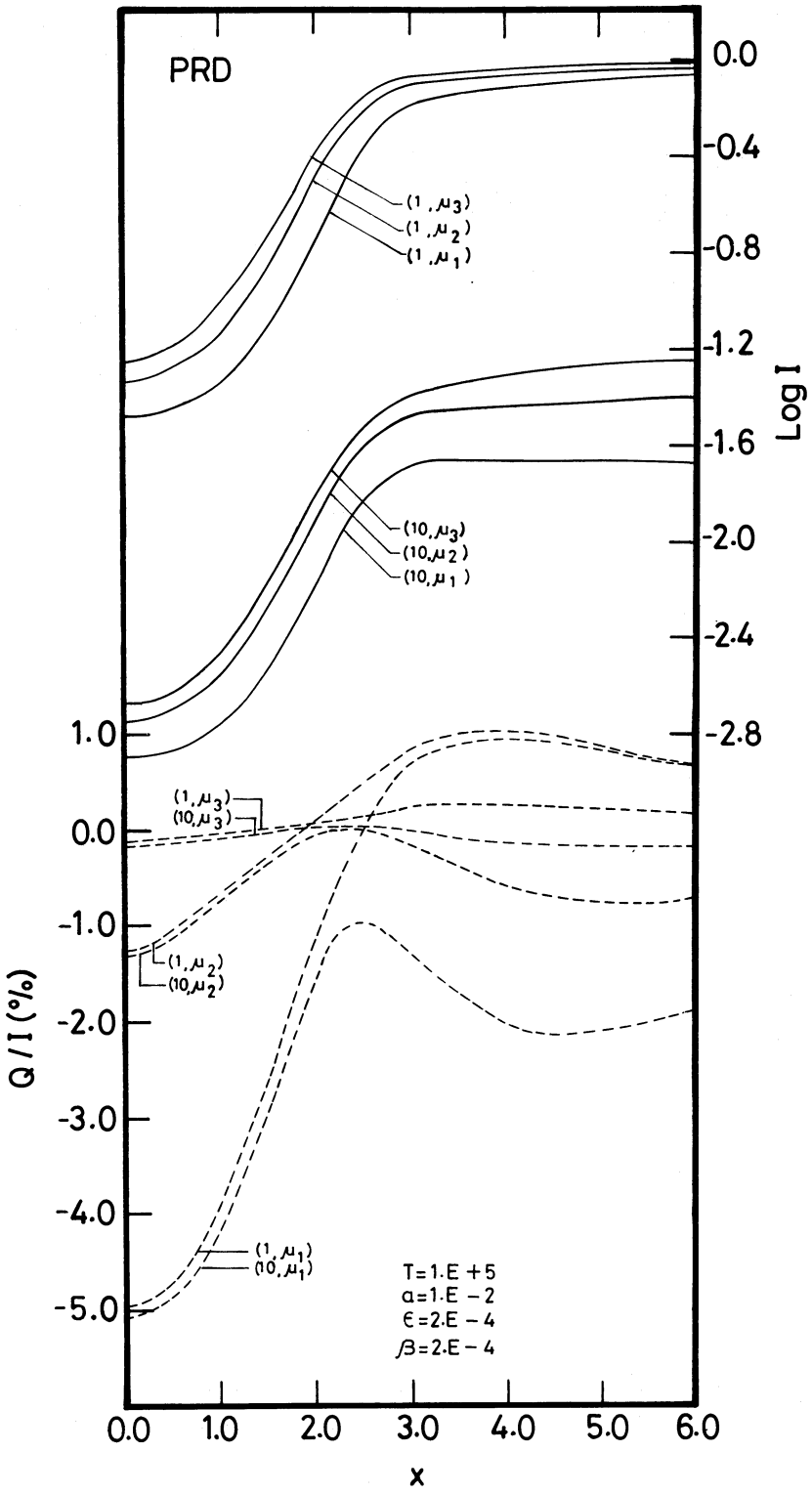

FIG. 11.—Same as Fig. 10, but for PRD scattering mechanism

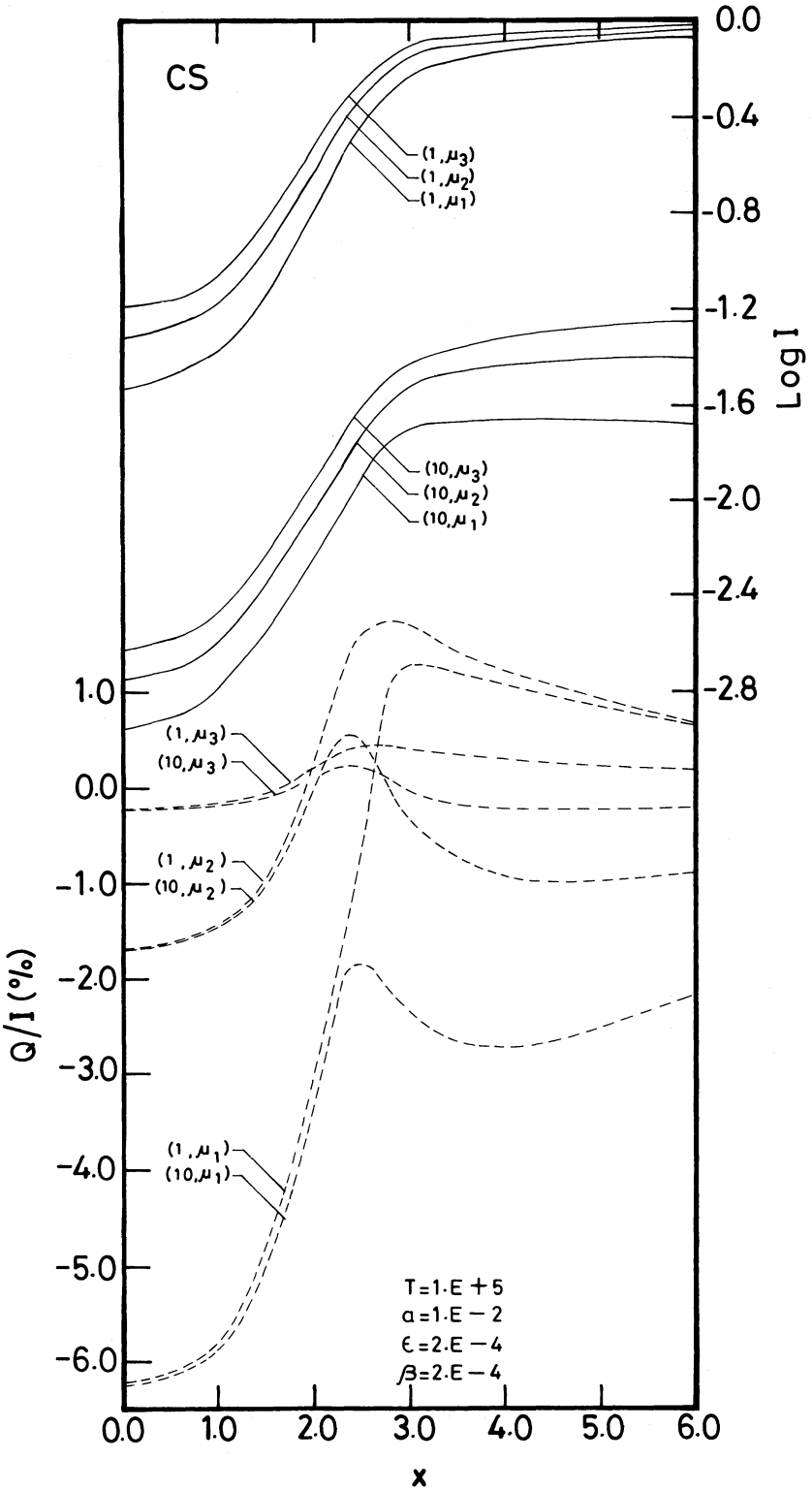

FIG. 12.—Angular dependence of the emergent I and Q/I profiles corresponding to the model of Figs. 8 and 9

whereas the CS polarization profiles are wider. Apart from the central peak, the other positive and negative polarization maxima in CS case occur nearer to the line core than in the PRD case. This is due to the nature of the redistribution functions themselves. This also indicates that PRD goes to CS only in the very far wings. The apparent similarity of CS and PRD polarization profiles in our figures is mainly because of too high a value of β we have selected for the models. The CRD polarization profiles significantly differ from CS polarization profiles both in magnitude and the shape in the line wings.

In Figure 13 we have shown another example of the comparison between CRD, PRD, and CS polarizations. This model is less extended ($R = 3$). The parameters $T = 10^7$ and $\beta = 7 \times 10^{-7}$ represent a strong line. In this case Hubený's condition, $\beta \ll a/\pi^2$, for the importance of PRD effects in the line wings in the presence of a continuous absorption is fairly well satisfied ($7 \times 10^{-7} \ll 10^{-5}$). Hence the PRD effects are not dominated over by the continuous absorption and emission. This model has a slightly different character than the earlier model. In fact, it resembles more the solution obtained for a semi-infinite atmosphere. From this point of view, it is useful just to compare the Figure 13 with the semi-infinite model profiles presented by Rees and Saliba (1982, their Figs. 4*a–b*). Our model is optically thick ($[aT]^{1/3} = 10$) and effectively very thick ($\epsilon T = 10^3$). The continuum absorption process (through β) destroys the line wing photons as far as the line radiation field is concerned. In this regard, it competes with the collisional de-excitation process (through ϵ) in the frequency thermalization of the source function. Frequency thermalization refers to the frequency diffusion (line wing to core) process which naturally operates in R_{II} partial redistribution mechanism, leading to the arrival of line wing photons at the core before escaping from the medium, where subsequent line scatterings can be well described by CRD. The frequency thermalization is very effective when line optical depths are large. To decide which of the two processes is stronger, we have to compare the characteristic depths τ_β, τ_ϵ (at characteristic frequencies) and characteristic frequencies x_β, x_ϵ (see Hubený 1985 for derivation and further details; see also Frisch 1980). The characteristic depth of frequency thermalization process is given by $\tau_{FT} = \min(\tau_\beta, \tau_\epsilon)$; $\tau_\beta \approx a^{-1/4}\beta^{-3/4}$; $\tau_\epsilon \approx a^{-1}\epsilon^{-3/2}$. For our model, $\tau_{FT} \approx \min(4.132 \times 10^5, 10^{10}) \approx 4.132 \times 10^5$. Also, the global behavior of source function is controlled by a thermalization length Λ, given by $\Lambda = \min(\tau_{th}, \tau_\beta)$; $\tau_{th} \sim \epsilon^{-1}$. For our model, $\Lambda \approx \min(10^4, 4.132 \times 10^5) \approx 10^4$. Hence our model satisfies $T \gg \Lambda$ and $T \gg \tau_{FT}$. Notice also that the frequency point beyond which the overlapping continuum dominates the total source function is given by $(\pi\beta/a)^{-1/2} \approx 6.743$ (Hubený 1985). The characteristic frequency of frequency thermalization is given by $x_{FT} = \min(x_\beta, x_\epsilon)$; $x_\beta \approx a^{1/4}\beta^{-1/4}$; $x_\epsilon \approx \epsilon^{-1/2}$. For our model, $x_{FT} \approx \min(3.4572, 100) \approx 3.4572$, which implies that the continuum radiation field begins to exceed the line radiation field around this frequency. At $x < x_{FT}$, the line radiation field is dominant, and the emergent radiation in particular behaves as though β is effectively very small. This is clearly seen in the CS intensity and polarization profiles. They are almost frequency independent in the line core (as they do for CS throughout the bandwidth when $\beta = 0$). Another point seen from Figure 13 is the insensitivity of polarization in this model to the geometry (PP and SS) in the line core. This is possibly due to the line being effectively very thick and to the relatively smaller extent of the atmosphere. Although there is a small difference in the behavior of linear polarization profiles of Figure 13 and those of Figures 10–12, qualitatively there is a similarity.

The effect of β on the polarization in the wings of resonance lines is substantial and strongly model dependent. Faurobert (1988) has studied in detail such problems, using PP semi-infinite atmospheres. It is important to note that the results presented in Figures 10–13 are continuum dominated, and the models are not fully suited for highlighting all aspects of the resonance line polarization, such as in a pure line case without continuum. However, the values of β we have used are quite common in stellar atmosphere model calculations. Because of such high values of β in these models, the CS solutions although being idealistic, behaved as well. I am grateful to the referee to have pointed out these two aspects of the results presented in this paper.

f) The Behavior of Resonance Line Polarization Profiles on the Disk of a Spherically Symmetric Atmosphere

The disk integrated polarization of a SS model is always zero. However, with recent advances in interferometric techniques it may be possible in future to resolve stellar disks and to measure intensity and polarization both in the lines and the continuum. The measurement of these quantities as a function of the impact parameter h (or in general different spatial points on the disk) at a given frequency point, say line center, etc. is of some theoretical interest. We have shown an example in Figures 14–16, taking CRD profiles. As usual, $k(r) = Kr^{-2}$ and $B'(r) = 1$. The angular dependence of I is quite strong in this case.

Figure 15 shows the distribution of intensity and polarization across the disk of the SS model whose radius R is 10 times that of the core radius $R_c(= 1)$. The stellar core emits a strong continuum radiation in the bandwidth of the line. The impact parameter h refers to the perpendicular distance of a line of sight from the line joining the center of the star to the observer (central ray). The $I(h)$ and $p(h)$ are shown across only one-half of the disk since there is a reflection symmetry about the central ray. All the frequency points in the line profile have almost same intensity for the lines of sight intersecting the core ($h < 1$). In other words, no line is formed across the geometric extension of the stellar core with respect to the central ray. The continuum is so strong that it fills the usual absorption line and saturates to the line wing intensity level existing in the layers nearer to the stellar core. The $I(h)$ for $x = 0$, 0.5, and 1 are almost independent of h. For frequency points $x > 1$, the limb darkening nature is clearly seen. As we go to higher and higher frequency points, the limb darkening becomes more and more severe. The degree of polarization $p(h)$ has a similar behavior. The polarization is maximum at the line center frequency point $x = 0$ and approaches zero in the line wing frequencies. The polarization is always negative and exhibits the expected behavior of maximum polarization at the limb of the disk. The polarization at the center of the disk is zero (e.g., the central ray). The polarization is almost zero for all the frequency points in the region where lines of sight intersect the stellar core. The polarization smoothly varies across the side lobe. In integrating the transfer equation along the line of sight rays, we have employed the angle and frequency-averaged source functions retaining just the polarization information. The polarization will show a stronger center to limb variation if these factors are explicitly included. Figure 15 gives just an idea of the polarization content of the diffuse radiation field across the disk.

Figure 16 shows the appearance of line profile $I(x)$ and polarization $p(x)$ at various impact parameters h. There is negligible difference at the line core. The emission at the wing continuously decrease across the disk, and in the outermost layer it becomes an emission line. The $p(x)$ profiles are not much different across the disk, except for a gradual increase in the polarization toward the stellar limb.

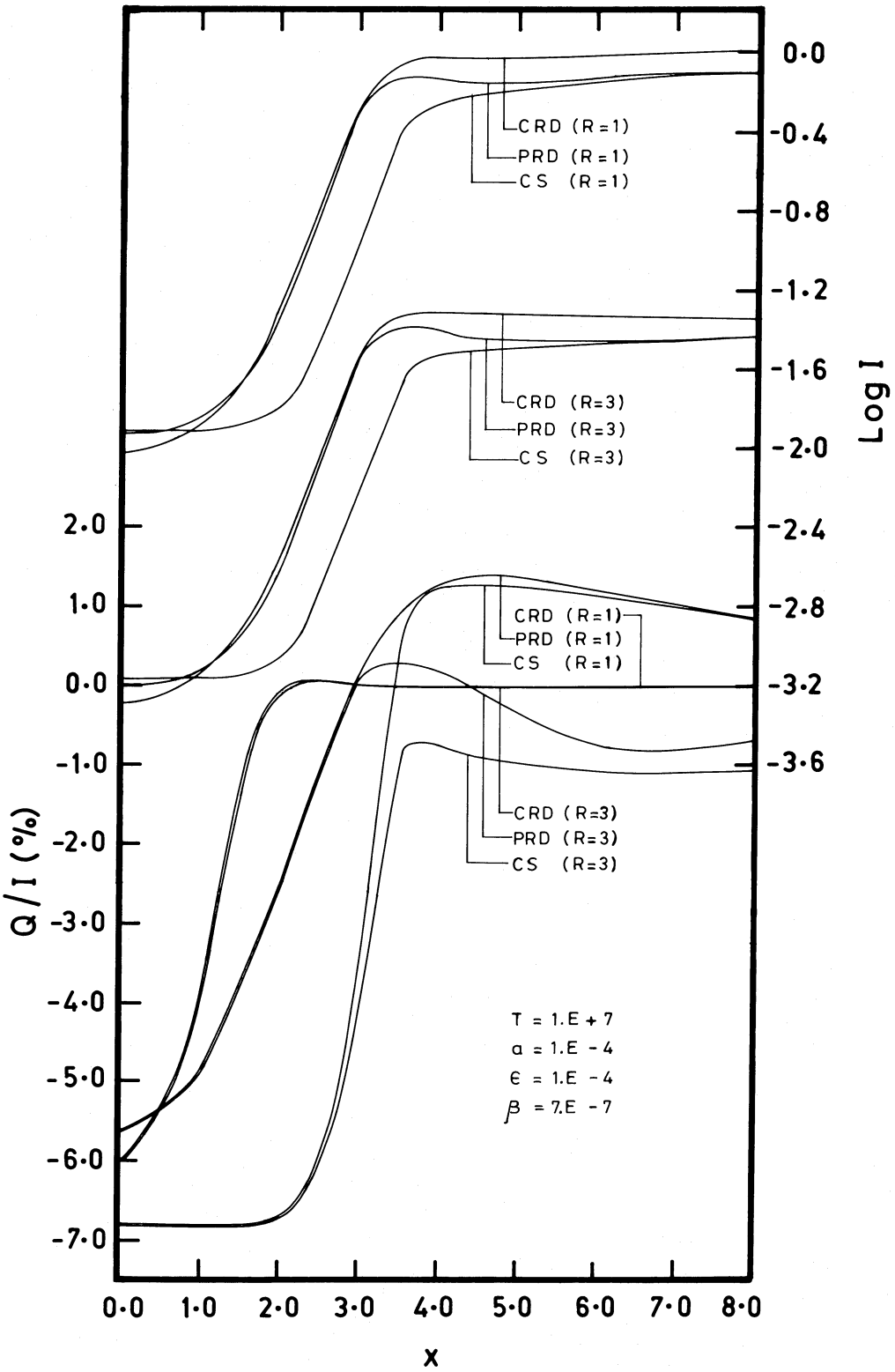

FIG. 13.—Comparison of CRD, PRD, and CS emergent intensity I and Q/I profiles in the direction $\mu_1 = 0.11$, for plane-parallel ($R = 1$) and spherically symmetric ($R = 3$) configurations. The model (T, a, ϵ, β) is given in the figure.

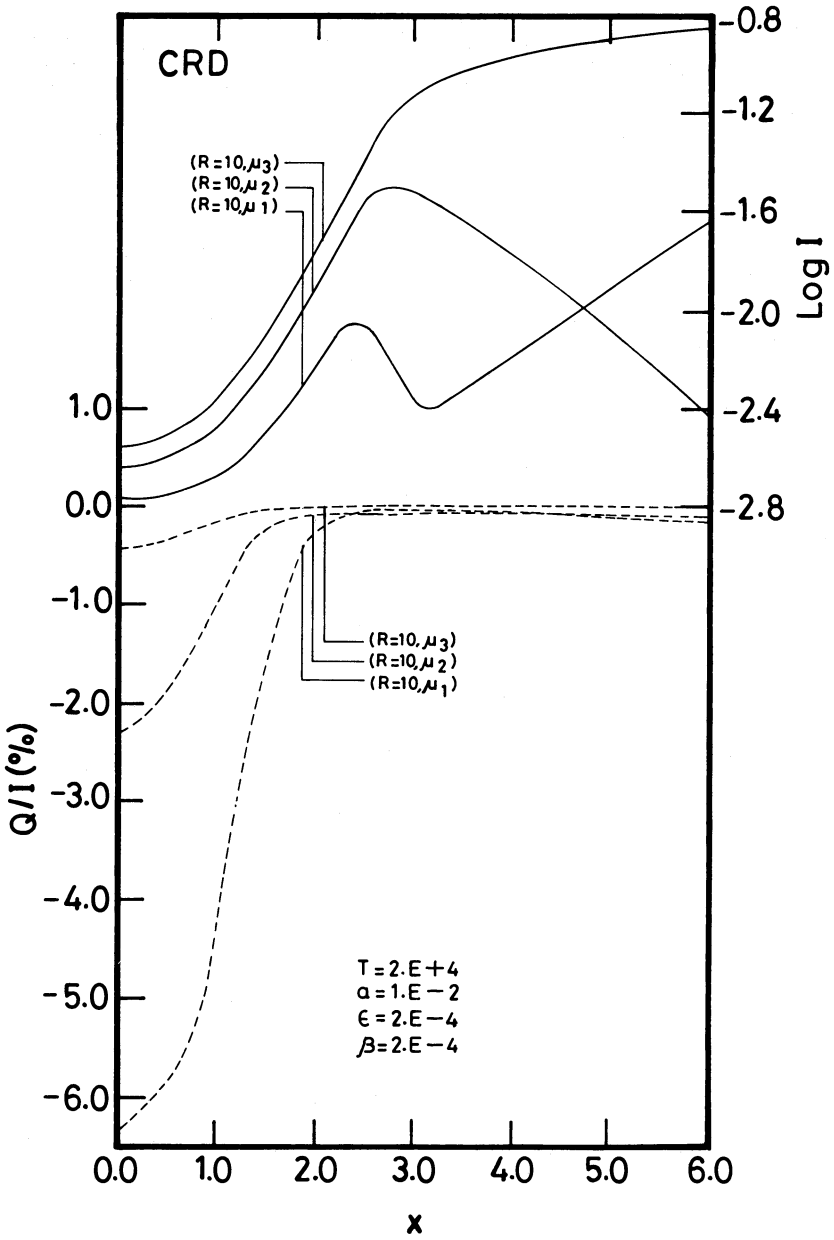

FIG. 14.—Angular dependence of emergent I and Q/I profiles for the model given in the figure

V. CONCLUSIONS

We have discussed some basic aspects of the resonance line polarization in spherically symmetric media. We have taken simple physical and atmospheric models for this purpose. Our aim has been to understand the two-level atom line polarization transfer in spherical geometry. It is found that the sphericity and extendedness substantially affect the polarization in the resonance line. It is seen that both CRD and PRD models of line scattering give correct description of the line core. However, in the line wings the PRD appears to be a better model in the plane-parallel situation, as shown by earlier works. We feel that this conclusion is valid even for wing polarization in spherically symmetric media. The computations are preliminary in nature and will be useful for getting a general idea about the resonance line polarization in moderately extended static spherical stellar atmospheres. The behavior of line polarization in expanding SS models is more complex, and its interpretation would be a nontrivial problem. The line of sight profiles and polarizations can be computed to a higher degree of completeness than presented here. This aspect, as well as the use of highly extended systems, is a topic which needs careful study since it represents a situation closer to the feasibility of future observations.

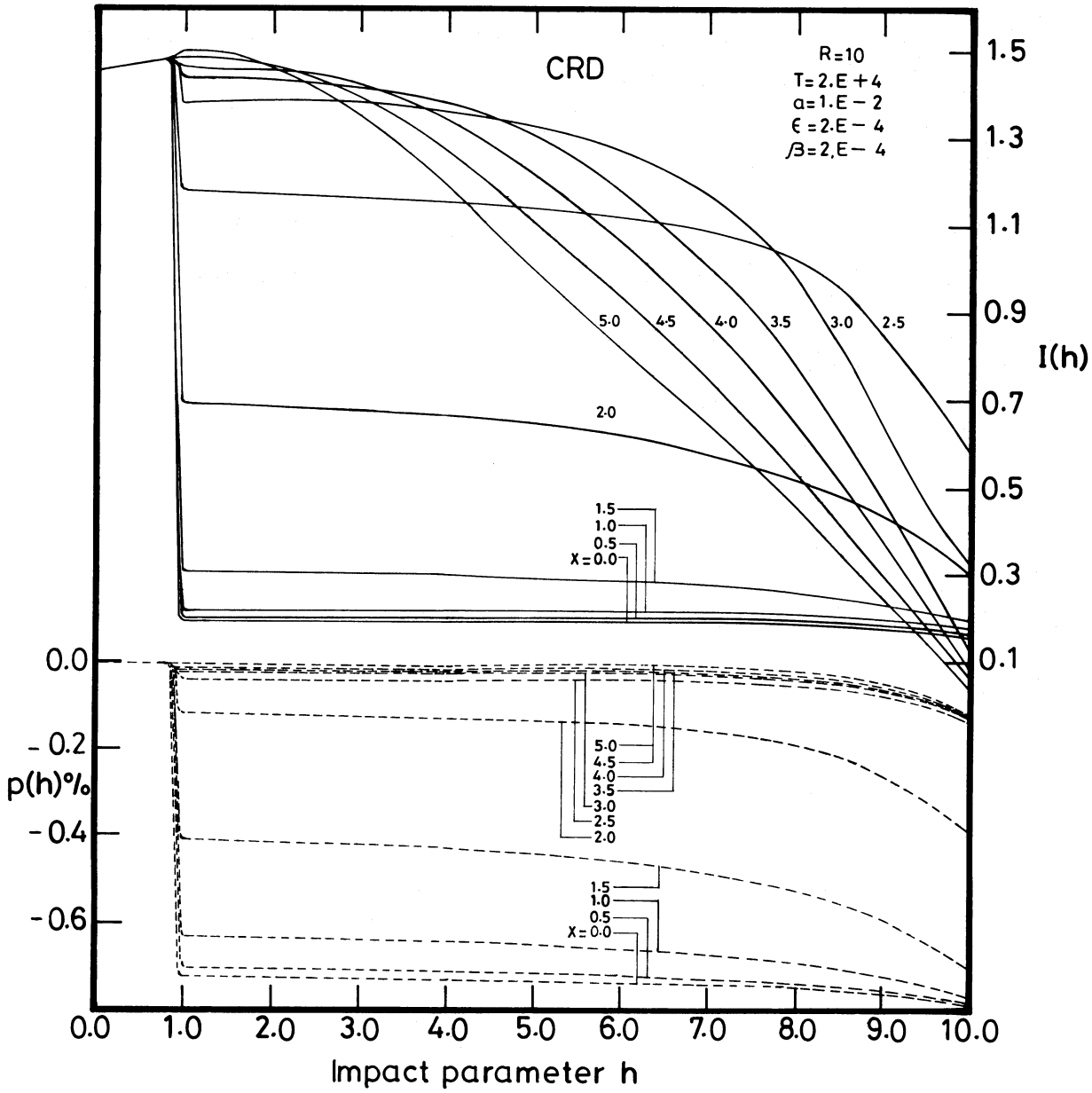

FIG. 15.—Distribution of intensity $I(h)$ and polarization $p(h)$ on the disk of an extended ($R = 10$) spherical atmosphere. See Fig. 14 also.

I am grateful to Professor A. Peraiah for helpful discussions on many aspects of the problem discussed in this paper. The numerical values of the published results in plane-parallel case were kindly provided by D. E. Rees and G. Saliba, which helped me in checking my computations. I am grateful to D. Mohan Rao for extensive discussions and critical comments. I am thankful to K. K. Ghosh for his help in the computations. I thank the referee for important suggestions.

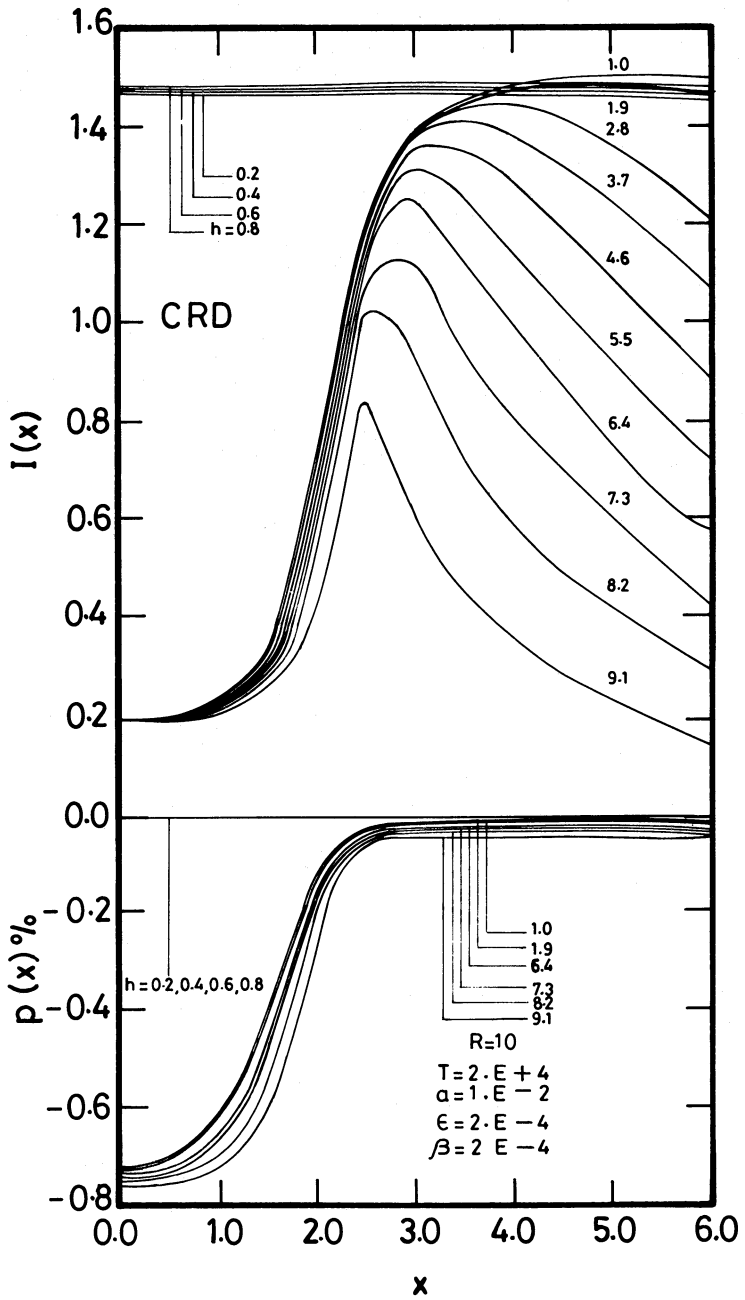

FIG. 16.—Appearance of the line intensity and polarization profiles at various impact parameters *h*. See Fig. 15 also.

REFERENCES

Auer, L. H., Rees, D. E., and Stenflo, J. O. 1980, *Astr. Ap.*, **88**, 302.
Chandrasekhar, S. 1960, *Radiative Transfer* (New York: Dover).
Dumont, S., Omont, A., and Pecker, J. C. 1973, *Solar Phys.*, **28**, 271.
Dumont, S., Omont, A., Pecker, J. C., and Rees, D. E. 1977, *Astr. Ap.*, **54**, 675.
Faurobert, M. 1987, *Astr. Ap.*, **178**, 269.
———. 1988, *Astr. Ap.*, **194**, 268.
Frisch, H. 1980, *Astr. Ap.*, **83**, 166.
Hubený, I. 1985, *Astr. Ap.*, **145**, 461.
Hummer, D. G. 1962, *M.N.R.A.S.*, **125**, 21.
Kunasz, P. B., and Hummer, D. G. 1974, *M.N.R.A.S.*, **166**, 19.
Landi degl'Innocenti, E. 1984, *Solar Phys.*, **91**, 1.
McKenna, S. J. 1984, *Ap. Space Sci.*, **106**, 283.
———. 1985, *Ap. Space Sci.*, **108**, 31.
Mihalas, D. 1978, *Stellar Atmospheres* (San Francisco: Freeman).
Mihalas, D., Kunasz, P. B., and Hummer, D. G. 1975, *Ap. J.*, **202**, 465.
Nagendra, K. N. 1987, *Astr. Nach.*, **308**, 303.
Nagendra, K. N., and Peraiah, A. 1985, *M.N.R.A.S.*, **214**, 203.
———. 1987, *Astr. Ap.*, **181**, 71.
Peraiah, A. 1984, in *Methods in Radiative Transfer*, ed. W. Kalkofen (Cambridge: Cambridge University Press), p. 281.
Rees, D. E., and Saliba, G. 1982, *Astr. Ap.*, **115**, 1.
Stenflo, J. O. 1976, *Astr. Ap.*, **46**, 61.
Stenflo, J. O., Bauer, T. G., and Elmore, D. F. 1980, *Astr. Ap.*, **84**, 60.
Stenflo, J. O., and Stenholm, L. 1976, *Astr. Ap.*, **46**, 69.

K. N. NAGENDRA: Indian Institute of Astrophysics, Bangalore 560 034, India